Published in final edited form as:

Science. 2022 March 25; 375(6587): 1373–1378. doi:10.1126/science.abm5561.

Architecture and antigenicity of the Nipah virus attachment glycoprotein

Zhaoqian Wang[1], **Moushimi Amaya**[2,3], **Amin Addetia**[1], **Ha V. Dang**[1], **Gabriella Reggiano**[1], **Lianying Yan**[2,3], **Andrew C. Hickey**[2,4], **Frank DiMaio**[1], **Christopher C. Broder**[2], **David Veesler**[1,5,*]

[1]Department of Biochemistry, University of Washington, Seattle, WA 98195, USA

[2]Department of Microbiology and Immunology, Uniformed Services University, Bethesda, Maryland, 20814, USA

[3]Henry M. Jackson Foundation for the Advancement of Military Medicine, Bethesda, MD 20814, USA

[4]U.S. Public Health Services Commissioned Corps, Rockville, MD 20852

[5]Howard Hughes Medical Institute, Seattle, WA 98195, USA.

Abstract

Nipah virus (NiV) and Hendra virus (HeV) are zoonotic henipaviruses (HNVs) responsible for outbreaks of encephalitis and respiratory illness. HNVs entry into host cells requires the attachment (G) and fusion (F) glycoproteins which are the main targets of antibody responses. To understand viral infection and host immunity, we determined a cryo-electron microscopy structure of the NiV G homotetrameric ectodomain in complex with the nAH1.3 broadly neutralizing antibody Fab fragment. We show that a cocktail of two non-overlapping G-specific antibodies neutralizes NiV and HeV synergistically and limits the emergence of escape mutants. Analysis of polyclonal serum antibody responses elicited by vaccination of macaques with NiV G indicates that the receptor-binding head domain is immunodominant. These results pave the way for implementing multi-pronged therapeutic strategies against these deadly pathogens.

Nipah virus (NiV) and Hendra virus (HeV) are bat-borne zoonotic pathogens of the *Henipavirus* (HNV) genus causing encephalitis and respiratory symptoms in humans with fatality rates between 50% and 100% (1). Over the past two decades, NiV has spilled over

*Correspondence: dveesler@uw.edu.

Author contributions: Z.W., M.A., A.A., H.V.D., C.C.B. and D.V. conceived the study. Z.W. and H.V.D designed NiV sG and head domain constructs and recombinantly expressed and purified them. L.Y. developed, characterized and produced the other recombinant tetrameric henipavirus sG glycoproteins. A.C.H. developed and characterized mAb nAH1.3. Z.W. and H.V.D. carried out biolayer interferometry binding assays. M.A. performed neutralization assays and viral antibody escape passaging. A.A. prepared libraries for deep sequencing and analyzed the data. Z.W. purified serum polyclonal antibodies and performed ELISA and depletion assays. Z.W. carried out cryoEM and negative stain EM sample preparation and data collection. Z.W. and D.V. processed the cryoEM data and built and refined atomic models. Z.W. and D.V. wrote the manuscript with input from all the authors. C.C.B. and D.V. acquired funding to support this study.

Competing interests: C.C.B is a United States federal employee and co-inventor on US and foreign patents pertaining to soluble forms of Nipah virus and Hendra virus G glycoproteins and C.C.B. and M.A. are co-inventors on US and foreign patents pertaining to Cedar virus and methods of use and recombinant Cedar virus chimeras, whose assignees are the US as represented by the Henry M. Jackson Foundation for the Advancement of Military Medicine (Bethesda, MD, USA).

into humans almost annually in Bangladesh (Bangladesh strain, NiV-B) (2) and has also caused outbreaks in India (NiV-B) and the Philippines (Malaysia strain, NiV-M) (3–5). The detection of cross-reactive HNVs antibodies (Abs) in humans and *Pteropus* bats in Africa underscored that 2 billion people worldwide live in regions threatened by HNV spillovers (6). Moreover, the recent discovery of a new HeV genotype (7, 8) is an urgent reminder of the HNV zoonotic threat. To date, no approved vaccines or therapeutics for use in people exist against HNV infections (9).

HNV entry into host cells requires fusion of the viral membrane and the host plasma membrane through the concerted action of an attachment (G) glycoprotein and a fusion (F) glycoprotein. The NiV and HeV entry receptors at the surface of host cells are the transmembrane protein tyrosine kinases ephrin-B2 or ephrin-B3 (10–13). G and F have been proposed to undergo a cascade of conformational changes to promote membrane fusion upon receptor engagement (14, 15). HNV G and F are the targets of the humoral immune response (16–19) and serum neutralizing antibodies (Abs) are a correlate of protection in animals experimentally infected with NiV or HeV (20–23). The cross-reactive NiV/HeV G-specific m102.4 monoclonal Ab (mAb) has been administered on an emergency compassionate use basis to 15 individuals with high risk exposure to HeV or NiV infection and recently completed a phase I clinical trial in Australia (24).

A soluble HeV G tetrameric ectodomain immunogen (HeV sG) elicits high titers of cross-reactive neutralizing Abs and protects against both NiV and HeV challenge in preclinical studies (20, 25–30). A vaccine using HeV sG is commercially available for use in horses in Australia (Equivac® HeV, Zoetis Inc.), and a formulation suitable for human use has recently entered phase I clinical trials (NCT04199169). Although crystal structures of the isolated NiV and HeV G head domains were previously determined (10, 13), no structural information is available for any HNV G tetramer, hindering both our understanding of immunity directed towards G and the rational design of improved vaccine candidates.

Results

Architecture of the NiV G tetramer

To unveil the 3D organization of the HNV G protein and provide a blueprint for vaccine design, we determined a cryoEM structure of the NiV G ectodomain homotetramer bound to the mouse nAH1.3 neutralizing antibody Fab fragment (31) at 3.5Å overall resolution (Figure S1). We used local refinement to account for the flexibility of the viral membrane proximal region relative to the distal region, yielding reconstructions at 3.5Å and 3.2Å resolution, respectively, allowing us to build a (composite) model of the NiV G ectodomain tetramer (Figure 1A-C, Figure S1 and Table S1). The final model comprises nearly the entire NiV sG ectodomain from residues 96 to 602 along with the nAH1.3 Fab variable domains. NiV G forms a 200Å long and 120Å wide intertwined homotetramer. At the core is an N-terminal 4-helix bundle (stalk) followed by an interlaced β-sandwich (designated neck) that connects to a C-terminal β-propeller head domain on each protomer (Figure 1A-C). The NiV G tetramer is stabilized by inter-protomer disulfide bonds formed in the neck and in the stalk (Figure 1D).

NiV G residues 96–147 form a pseudo 2-fold symmetric helical bundle, which is presumably extended at its N-terminal end towards the viral membrane in which the tetramer is anchored (residues 70–95 are weakly resolved in the cryoEM map and were not modeled) (Figure 1A-C). The interlaced β-sandwich neck domain is formed by apposition of two 4-stranded mixed β-sheets, packed against each other through hydrophobic contacts, comprising residues 153–163 from each of the four protomers (Figure 1D). The neck is covalently cross-linked through formation of two antiparallel inter-protomer disulfide bonds between residues C158 and C162 of chains A and D and two antiparallel disulfides between residues C158 and C162 of chains B and C. The neck is decorated with four N-linked glycans protruding from residue N159 on each protomer, partially shielding this domain on both sides of the β-sandwich (Figure 1D). Each of the four C-terminal head domains form a 6-bladed β-propeller decorated with five N-linked oligosaccharides at positions N306, N378, N417, N481 and N529, which are all resolved in the cryoEM map (Figure 1A-C). Two head domains are connected to the neck through flexible linkers folding back towards the viral membrane with the β-propellers docked on either side of the stalk (Figure 1B-C). The other two head domains form a head-to-tail dimer positioned distal to the viral membrane and are connected to the neck through linkers that adopt distinct folds (Fig 1B-C). As a result, the NiV G tetramer is assembled from four identical polypeptides adopting three distinct folding patterns (Fig 1E). Interactions between the two distal head domains maintain their approximately antiparallel orientation whereas contacts between each proximal head and the NiV G stalk lead to their pseudo-2-fold symmetrical arrangement. Only one out of four head domains orients its receptor-binding site towards the host cell surface whereas the other three sites point towards the viral membrane (Fig 1F), suggesting that conformational dynamics would allow reorienting the head domains for receptor engagement. Although the cryoEM map does not resolve the topology of the two stalk C146 disulfide bonds unambiguously, previous biochemical data suggest they form across pairs of protomers that are not covalently cross-linked in the neck (25, 32). The overall NiV G architecture described here adopts a unique two heads up and two heads down conformation that is different from structures of any other paramyxovirus attachment glycoproteins. As a comparison, Newcastle disease virus HN adopts a four heads down conformation whereas parainfluenza virus 5 HN exhibits a distinct two heads up and two heads down conformation with the receptor binding sites oriented differently than for NiV G (33, 34) (Figure S2).

nAH1.3-mediated broad neutralization of NiV and HeV

The nAH1.3 mAb was previously shown to potently neutralize NiV-M, NiV-B and HeV in vitro (31). Using a green fluorescent protein (GFP)-encoding, replication-competent, Cedar (henipa)virus (rCedV) chimeras in which the native glycoproteins are substituted with the NiV-B (rCedV-NiV-B-GFP) or the HeV (rCedV-HeV-GFP) F and G glycoproteins (35), we determined nAH1.3 half-maximum inhibitory concentrations (IC_{50}) of 33 ng/mL and 32 ng/mL, respectively (Figure S3A). This neutralization potency is comparable to the human mAb m102.4 for which we determined IC_{50} values of 17 ng/mL and 58 ng/mL against rCedV-NiV-B-GFP and rCedV-HeV-GFP, respectively (Figure S3B). Our cryoEM structure reveals that one nAH1.3 Fab fragment is bound to each NiV G head domain (Figure 1B-C and Figure 2A). nAH1.3 heavy and light chains interact with an antigenic site located on the side of the β-propeller that is opposite to the ephrin-B2/B3-binding site (Figure 2A).

As a result, nAH1.3 does not compete with receptor binding to the NiV G ectodomain (Figure 2B), unlike m102.4 which forms interactions mimicking receptor interactions (18). nAH1.3 buries ~1,000 $Å^2$ of its paratope upon binding through shape complementarity and hydrogen bonding involving complementary determining regions (CDR) H1, H3, L1 and L2, explaining its high affinity binding to NiV G (Figure 2C-D and Figure S3C). nAH1.3 is conformation-dependent and recognizes a discontinuous epitope, spanning residues 172, 182–191, 358, 448–451, 468–478, 515–518 and 570–571, which is in close proximity to the oligosaccharide at position N481 (Figure 1A and Figure 2A). 21 out of 26 epitope residues are strictly conserved across NiV G and HeV G and 3 residues are conservatively substituted from NiV G to HeV G (N187Q, N478Q and I517L). Only 2 residues are non-conservatively substituted (L470D and K571V and these map to the periphery of the epitope (Fig 2E). Our structural data suggest that none of the 5 substitutions would affect nAH1.3 recognition, as confirmed by the similar neutralization potencies determined against rCedV-NiV-B-GFP and rCedV-HeV-GFP (Figure S3A). However, no cross-reactivity was detected with more divergent HNV sG ectodomain tetramers from CedV, Ghana virus (GhV) and Mojiang virus (MojV) (Figure S3D–E). Since mAb nAH1.3 does not appear to affect the overall NiV G conformation (36) nor to bind to the ephrin virus entry receptor binding site, we propose that the mAb inhibits HNV entry into cells by interfering with its F fusion triggering mechanism, as supported by membrane fusion assays (37).

To validate our structural data, we passaged chimeric rCedV-NiV-B-GFP and rCedV-HeV-GFP in the presence of a sub-neutralizing concentration of nAH1.3. Deep sequencing revealed the selection of a clone harboring the I520T mutation (T1559C nucleotide substitution) introducing an N-linked glycosylation site at position N518 of NiV G. This is within the epitope recognized by nAH1.3 and likely abrogates mAb binding and neutralization via steric hindrance (Figure 2F and Figure S4A). For HeV G, we identified the T117A/N186D escape mutations. The latter substitution resides within the epitope and likely disrupts interactions with the nAH1.3 light chain (Figure 2D,F and Figure S4B). Previously identified Q450K and R516K nAH1.3 escape mutations (31), further validate our structure as both residues form extensive interactions with the Fab heavy chain (Figure 2F). Moreover, passaging of rCedV-HeV-GFP in the presence of m102.4 led to the emergence of a single amino acid mutation in HeV G (D582N) (Figure S4C) which is identical to the one previously identified using authentic HeV and NiV (31), validating the use of the chimeras as a surrogate system for pathogenic henipaviruses.

Synergistic neutralization of NiV and HeV by a mAb cocktail

mAb cocktails have had success in preventing or treating infections with RNA viruses (38). For instance, although the individual Regeneron 10933 (casirivimab) and 10987 (imdevimab) mAbs against SARS-CoV-2 are affected by a range of residue substitutions detected in clinical isolates, the two-mAb cocktail proved more resilient to escape mutations (39, 40). Because experimental passaging of NiV and HeV with low concentrations of neutralizing mAbs can favor the emergence of neutralization escape mutants, we tested a cocktail of m102.4 and nAH1.3 which recognize epitopes located on opposite sides of the β-propeller (Figure 3A). Analysis of the negatively stained complex between NiV G and the nAH1.3 and m102.4 Fabs by single particle analysis confirmed formation of

a ternary complex (Figure S5A–C), allowing the determination of a 3D reconstruction with three nAH1.3 and three m102.4 Fabs bound to a NiV G tetramer (Figure S5C). We subsequently used biolayer interferometry to confirm that both mAbs can recognize the NiV G ectodomain immobilized at the surface of biosensors irrespective of their order of addition (Fig 3B). We then carried out virus neutralization assays using rCedV-NiV-B-GFP or rCedV-HeV-GFP to examine whether these mAbs possessed synergistic virus-neutralizing activity (35). Using a concentration matrix of each mAb, we found that combining m102.4 and nAH1.3 led to synergistic neutralization of the two rCedV chimeras (Figure 3C-D and Figure S6A–B). Passaging chimeric rCedV-HeV-GFP in the presence of the cocktail of nAH1.3 and m102.4 led to the emergence of the T117A, N186D and T507I triple mutant with T507I mapping to the m102.4 epitope and N186D to the nAH1.3 epitope, as described above (Figure 2D,F and Figure S4D). These findings support the potential use of a cocktail of these two non-competing G glycoprotein-directed neutralizing mAbs as a therapeutic against these two deadly HNVs due to their synergy and the higher barrier for resistance due to the requirement for multiple mutations to escape neutralization.

The NiV G head domain is the main target of vaccine-elicited serum neutralizing activity

We next investigated the nature and fine-specificity of polyclonal Ab responses against the NiV G and HeV G glycoprotein using sera from two rhesus macaques that were immunized three times (4 weeks apart) with 200 μg of an alum-adjuvanted equimolar mixture of the purified NiV-B and NiV-M sG tetramers (Figure 4A). The two immunizations elicited potent serum neutralizing activity at day 84 with geometric mean neutralization titers of 1/8,434 and 1/992 against rCedV-NiV-B-GFP and rCedV-HeV-GFP, respectively (Figure 4B). Using competition ELISA with the nAH1.3 (31), m102.4 (42) and HENV-32 (43) mAbs, we showed that vaccine-elicited Abs target at least three distinct antigenic sites at the surface of the NiV G head domain with comparable magnitudes, illustrating the diversity of polyclonal Ab responses elicited by vaccination (Figure 4C-E). To directly visualize the epitopes recognized by serum Abs, we used single particle electron microscopy analysis of negatively stained complexes formed between NiV G and purified polyclonal Fab fragments (obtained from IgG cleavage) after size-exclusion chromatography (44–46). 3D classification of the data led to the identification of at least three distinct classes of head binding Abs and one class of stalk-specific Ab (Figure 4F-J and Figure S5D–F). Overall, Ab responses are virtually exclusively directed to the NiV G head domain, in spite of using the full ectodomain tetramer for immunization, underscoring an apparent focusing of Ab responses on the receptor-binding domain (Figure 4F-J and Figure S5D–F).

To understand the quantitative contribution of the different NiV G domains to serum neutralizing activity induced by vaccination, we depleted polyclonal Abs using either the purified isolated NiV G head domain or the tetrameric NiV G ectodomain. Neutralizing Ab titers for each of the two rhesus macaques were reduced 9 and 19-fold against rCedV-NiV-B-GFP (Figure 4K and Figure S6C–F) and 9 and 93-fold against rCedV-HeV-GFP (Figure 4L and Figure S6G–H) following depletion of NiV G head-specific Abs. Serum Ab depletion using the NiV G ectodomain tetramer resulted in a 11 and 13-fold dampening of neutralizing activity against rCedV-NiV-B-GFP (Figure 4K and Figure S6I–L) and a 69 and 2.5-fold reduction against rCedV-HeV-GFP (Figure 4L and Figure S6M–N). Collectively,

these data indicate that the NiV G head domain is immunodominant and the target of most serum neutralizing activity elicited by NiV G vaccination in rhesus macaques.

Discussion

Our structure of the NiV G ectodomain tetramer reveals the ultrastructural organization of this key target of the immune system, informs the mechanism of HNV entry into host cells and provides a blueprint for engineering next-generation vaccine candidates with improved stability and immunogenicity, as was successful for respiratory syncytial virus (47, 48) and SARS-CoV-2 (49–55). The discovery that the NiV/HeV G head domain is the target of most neutralizing activity in the serum of rhesus macaques vaccinated with tetrameric NiV G ectodomains motivates the development of vaccines focusing Ab responses on this domain of vulnerability. Presenting the head antigen as an ordered array through multivalent display bears the promise of enhancing immunogenicity, as recently described for SARS-CoV-2 (51, 56, 57), and would allow presentation of a mosaic of HNV head domains with the goal of inducing neutralizing Ab responses with maximal breadth (45, 57–59). Finally, the enhanced expression yield, stability and homogeneity of the NiV G head domain compared to HeV sG (35) would improve scalability of the manufacturing process of such a vaccine.

Supplementary Material

Refer to Web version on PubMed Central for supplementary material.

Acknowledgements:

This study was supported by the National Institute of Allergy and Infectious Diseases (DP1AI158186 and HHSN272201700059C to D.V., AI077995 to C.C.B. and U19AI142764 to C.C.B. and D.V.), the National Institute of Health Cellular and Molecular Biology Training Grant (T32GM007270 to A.A.), a Pew Biomedical Scholars Award (D.V.), an Investigators in the Pathogenesis of Infectious Disease Awards from the Burroughs Wellcome Fund (D.V.), the University of Washington Arnold and Mabel Beckman cryoEM center and the National Institute of Health grant S10OD032290 (to D.V.). The authors thank Auro Vaccines, LLC, for providing the rhesus macaque NiV-M and NiV-B sG immune sera, and also acknowledge the Coalition for Epidemic Preparedness Innovations (CEPI) for their support of the Nipah virus vaccine program. Molecular graphics and analyses performed with UCSF ChimeraX, developed by the Resource for Biocomputing, Visualization, and Informatics at the University of California, San Francisco, with support from National Institutes of Health R01-GM129325 and the Office of Cyber Infrastructure and Computational Biology, National Institute of Allergy and Infectious Diseases. The opinions and assertions expressed herein are those of the author(s) and do not necessarily reflect the official policy or position of the Uniformed Services University or the Department of Defense, or the Henry M. Jackson Foundation for the Advancement of Military Medicine, Inc. D.V is an Investigator of the Howard Hughes Medical Institute.

Data and Materials Availability.

The cryoEM maps and coordinates have been deposited to the Electron Microscopy Databank and Protein Data Bank with accession numbers listed in Table S1. Materials generated in this study will be made available on request after signing a materials transfer agreement with the University of Washington (Uniform Biological MTA).

References

1. Eaton BT, Broder CC, Middleton D, Wang LF, Hendra and Nipah viruses: different and dangerous. Nat. Rev. Microbiol 4, 23–35 (2006). [PubMed: 16357858]

2. Gurley ES, Hegde ST, Hossain K, Sazzad HMS, Hossain MJ, Rahman M, Sharker MAY, Salje H, Islam MS, Epstein JH, Khan SU, Kilpatrick AM, Daszak P, Luby SP, Convergence of Humans, Bats, Trees, and Culture in Nipah Virus Transmission, Bangladesh. Emerg. Infect. Dis 23, 1446–1453 (2017). [PubMed: 28820130]

3. Arunkumar G, Chandni R, Mourya DT, Singh SK, Sadanandan R, Sudan P, Bhargava B, People, Nipah Nipah Investigators, Health, Outbreak investigation of Nipah Virus Disease in Kerala, India, 2018. J. Infect. Dis (2018), doi:10.1093/infdis/jiy612.

4. Chadha MS, Comer JA, Lowe L, Rota PA, Rollin PE, Bellini WJ, Ksiazek TG, Mishra A, Nipah virus-associated encephalitis outbreak, Siliguri, India. Emerg. Infect. Dis 12, 235–240 (2006). [PubMed: 16494748]

5. Ching PK, de los Reyes VC, Sucaldito MN, Tayag E, Columna-Vingno AB, Malbas FF Jr., Bolo GC Jr., Sejvar JJ, Eagles D, Playford G, Dueger E, Kaku Y, Morikawa S, Kuroda M, Marsh GA, McCullough S, Foxwell AR, Outbreak of henipavirus infection, Philippines, 2014. Emerg. Infect. Dis 21, 328–331 (2015). [PubMed: 25626011]

6. Pernet O, Schneider BS, Beaty SM, LeBreton M, Yun TE, Park A, Zachariah TT, Bowden TA, Hitchens P, Ramirez CM, Daszak P, Mazet J, Freiberg AN, Wolfe ND, Lee B, Evidence for henipavirus spillover into human populations in Africa. Nat. Commun 5, 5342 (2014). [PubMed: 25405640]

7. Annand EJ, Horsburgh BA, Xu K, Reid PA, Poole B, de Kantzow MC, Brown N, Tweedie A, Michie M, Grewar JD, Jackson AE, Singanallur NB, Plain KM, Tachedjian M, van der Heide B, Williams DT, Secombe C, Laing ED, Sterling S, Yan L, Jackson L, Jones C, Plowright RK, Peel AJ, Diallo I, Breed AC, Broder CC, Britton PN, Dhand NK, Smith I, Eden J-S, Novel Hendra virus variant detected by sentinel surveillance of Australian horses. bioRxiv (2021), p. 2021.07.16.452724.

8. Wang J, Anderson DE, Halpin K, Hong X, Chen H, Walker S, Valdeter S, van der Heide B, Neave MJ, Bingham J, O'Brien D, Eagles D, Wang L-F, Williams DT, A new Hendra virus genotype found in Australian flying foxes. Virol. J 18, 197 (2021). [PubMed: 34641882]

9. Amaya M, Broder CC, Vaccines to Emerging Viruses: Nipah and Hendra. Annu Rev Virol 7, 447–473 (2020). [PubMed: 32991264]

10. Xu K, Rajashankar KR, Chan YP, Himanen JP, Broder CC, Nikolov DB, Host cell recognition by the henipaviruses: crystal structures of the Nipah G attachment glycoprotein and its complex with ephrin-B3. Proc. Natl. Acad. Sci. U. S. A 105, 9953–9958 (2008). [PubMed: 18632560]

11. Bonaparte MI, Dimitrov AS, Bossart KN, Crameri G, Mungall BA, Bishop KA, Choudhry V, Dimitrov DS, Wang LF, Eaton BT, Broder CC, Ephrin-B2 ligand is a functional receptor for Hendra virus and Nipah virus. Proc. Natl. Acad. Sci. U. S. A 102, 10652–10657 (2005). [PubMed: 15998730]

12. Negrete OA, Levroney EL, Aguilar HC, Bertolotti-Ciarlet A, Nazarian R, Tajyar S, Lee B, EphrinB2 is the entry receptor for Nipah virus, an emergent deadly paramyxovirus. Nature. 436, 401–405 (2005). [PubMed: 16007075]

13. Bowden TA, Aricescu AR, Gilbert RJ, Grimes JM, Jones EY, Stuart DI, Structural basis of Nipah and Hendra virus attachment to their cell-surface receptor ephrin-B2. Nat. Struct. Mol. Biol 15, 567–572 (2008). [PubMed: 18488039]

14. Liu Q, Stone JA, Bradel-Tretheway B, Dabundo J, Benavides Montano JA, Santos-Montanez J, Biering SB, Nicola AV, Iorio RM, Lu X, Aguilar HC, Unraveling a three-step spatiotemporal mechanism of triggering of receptor-induced Nipah virus fusion and cell entry. PLoS Pathog 9, e1003770 (2013). [PubMed: 24278018]

15. Liu Q, Bradel-Tretheway B, Monreal AI, Saludes JP, Lu X, Nicola AV, Aguilar HC, Nipah virus attachment glycoprotein stalk C-terminal region links receptor binding to fusion triggering. J. Virol 89, 1838–1850 (2015). [PubMed: 25428863]

16. Dang HV, Cross RW, Borisevich V, Bornholdt ZA, West BR, Chan Y-P, Mire CE, Da Silva SC, Dimitrov AS, Yan L, Amaya M, Navaratnarajah CK, Zeitlin L, Geisbert TW, Broder CC, Veesler D, Broadly neutralizing antibody cocktails targeting Nipah virus and Hendra virus fusion glycoproteins. Nat. Struct. Mol. Biol 28, 426–434 (2021). [PubMed: 33927387]

17. Dang HV, Chan YP, Park YJ, Snijder J, Da Silva SC, Vu B, Yan L, Feng YR, Rockx B, Geisbert TW, Mire CE, Broder CC, Veesler D, An antibody against the F glycoprotein inhibits Nipah and Hendra virus infections. Nat. Struct. Mol. Biol (2019), doi:10.1038/s41594-019-0308-9.

18. Xu K, Rockx B, Xie Y, DeBuysscher BL, Fusco DL, Zhu Z, Chan Y-P, Xu Y, Luu T, Cer RZ, Feldmann H, Mokashi V, Dimitrov DS, Bishop-Lilly KA, Broder CC, Nikolov DB, Crystal structure of the Hendra virus attachment G glycoprotein bound to a potent cross-reactive neutralizing human monoclonal antibody. PLoS Pathog 9, e1003684 (2013). [PubMed: 24130486]

19. Avanzato VA, Oguntuyo KY, Escalera-Zamudio M, Gutierrez B, Golden M, Kosakovsky Pond SL, Pryce R, Walter TS, Seow J, Doores KJ, Pybus OG, Munster VJ, Lee B, Bowden TA, A structural basis for antibody-mediated neutralization of Nipah virus reveals a site of vulnerability at the fusion glycoprotein apex. Proc. Natl. Acad. Sci. U. S. A (2019), doi:10.1073/pnas.1912503116.

20. Bossart KN, Rockx B, Feldmann F, Brining D, Scott D, LaCasse R, Geisbert JB, Feng YR, Chan YP, Hickey AC, Broder CC, Feldmann H, Geisbert TW, A Hendra virus G glycoprotein subunit vaccine protects African green monkeys from Nipah virus challenge. Sci. Transl. Med 4, 146ra107 (2012).

21. Bossart KN, Zhu Z, Middleton D, Klippel J, Crameri G, Bingham J, McEachern JA, Green D, Hancock TJ, Chan YP, Hickey AC, Dimitrov DS, Wang LF, Broder CC, A neutralizing human monoclonal antibody protects against lethal disease in a new ferret model of acute nipah virus infection. PLoS Pathog 5, e1000642 (2009). [PubMed: 19888339]

22. Geisbert TW, Mire CE, Geisbert JB, Chan YP, Agans KN, Feldmann F, Fenton KA, Zhu Z, Dimitrov DS, Scott DP, Bossart KN, Feldmann H, Broder CC, Therapeutic treatment of Nipah virus infection in nonhuman primates with a neutralizing human monoclonal antibody. Sci. Transl. Med 6, 242ra82 (2014).

23. Mire CE, Chan YP, Borisevich V, Cross RW, Yan L, Agans KN, Dang HV, Veesler D, Fenton KA, Geisbert TW, Broder CC, A Cross-Reactive Humanized Monoclonal Antibody Targeting Fusion Glycoprotein Function Protects Ferrets Against Lethal Nipah Virus and Hendra Virus Infection. J. Infect. Dis (2019), doi:10.1093/infdis/jiz515.

24. Playford EG, Munro T, Mahler SM, Elliott S, Gerometta M, Hoger KL, Jones ML, Griffin P, Lynch KD, Carroll H, Others, Safety, tolerability, pharmacokinetics, and immunogenicity of a human monoclonal antibody targeting the G glycoprotein of henipaviruses in healthy adults: a first-in-human, randomised, controlled, phase 1 study. Lancet Infect. Dis 20, 445–454 (2020). [PubMed: 32027842]

25. Bossart KN, Crameri G, Dimitrov AS, Mungall BA, Feng Y-R, Patch JR, Choudhary A, Wang L-F, Eaton BT, Broder CC, Receptor binding, fusion inhibition, and induction of cross-reactive neutralizing antibodies by a soluble G glycoprotein of Hendra virus. J. Virol 79, 6690–6702 (2005). [PubMed: 15890907]

26. Mungall BA, Middleton D, Crameri G, Bingham J, Halpin K, Russell G, Green D, McEachern J, Pritchard LI, Eaton BT, Wang L-F, Bossart KN, Broder CC, Feline model of acute nipah virus infection and protection with a soluble glycoprotein-based subunit vaccine. J. Virol 80, 12293–12302 (2006). [PubMed: 17005664]

27. McEachern JA, Bingham J, Crameri G, Green DJ, Hancock TJ, Middleton D, Feng Y-R, Broder CC, Wang L-F, Bossart KN, A recombinant subunit vaccine formulation protects against lethal Nipah virus challenge in cats. Vaccine. 26, 3842–3852 (2008). [PubMed: 18556094]

28. Pallister J, Middleton D, Wang L-F, Klein R, Haining J, Robinson R, Yamada M, White J, Payne J, Feng Y-R, Chan Y-P, Broder CC, A recombinant Hendra virus G glycoprotein-based subunit vaccine protects ferrets from lethal Hendra virus challenge. Vaccine. 29, 5623–5630 (2011). [PubMed: 21689706]

29. Mire CE, Geisbert JB, Agans KN, Feng Y-R, Fenton KA, Bossart KN, Yan L, Chan Y-P, Broder CC, Geisbert TW, A recombinant Hendra virus G glycoprotein subunit vaccine protects nonhuman primates against Hendra virus challenge. J. Virol 88, 4624–4631 (2014). [PubMed: 24522928]

30. Middleton D, Pallister J, Klein R, Feng Y-R, Haining J, Arkinstall R, Frazer L, Huang J-A, Edwards N, Wareing M, Elhay M, Hashmi Z, Bingham J, Yamada M, Johnson D, White J, Foord A, Heine HG, Marsh GA, Broder CC, Wang L-F, Hendra virus vaccine, a one health approach to protecting horse, human, and environmental health. Emerg. Infect. Dis 20, 372–379 (2014). [PubMed: 24572697]

31. Borisevich V, Lee B, Hickey A, DeBuysscher B, Broder CC, Feldmann H, Rockx B, Escape From Monoclonal Antibody Neutralization Affects Henipavirus Fitness In Vitro and In Vivo. J. Infect. Dis 213, 448–455 (2016). [PubMed: 26357909]
32. Maar D, Harmon B, Chu D, Schulz B, Aguilar HC, Lee B, Negrete OA, Cysteines in the stalk of the nipah virus G glycoprotein are located in a distinct subdomain critical for fusion activation. J. Virol 86, 6632–6642 (2012). [PubMed: 22496210]
33. Welch BD, Yuan P, Bose S, Kors CA, Lamb RA, Jardetzky TS, Structure of the parainfluenza virus 5 (PIV5) hemagglutinin-neuraminidase (HN) ectodomain. PLoS Pathog 9, e1003534 (2013). [PubMed: 23950713]
34. Yuan P, Swanson KA, Leser GP, Paterson RG, Lamb RA, Jardetzky TS, Structure of the Newcastle disease virus hemagglutinin-neuraminidase (HN) ectodomain reveals a four-helix bundle stalk. Proc. Natl. Acad. Sci. U. S. A 108, 14920–14925 (2011). [PubMed: 21873198]
35. Doyle MP, Kose N, Borisevich V, Binshtein E, Amaya M, Nagel M, Annand EJ, Armstrong E, Bombardi R, Dong J, Schey KL, Broder CC, Zeitlin L, Kuang EA, Bornholdt ZA, West BR, Geisbert TW, Cross RW, Crowe JE Jr, Cooperativity mediated by rationally selected combinations of human monoclonal antibodies targeting the henipavirus receptor binding protein. Cell Rep 36, 109628 (2021). [PubMed: 34469726]
36. Wong JJW, Young TA, Zhang J, Liu S, Leser GP, Komives EA, Lamb RA, Zhou ZH, Salafsky J, Jardetzky TS, Monomeric ephrinB2 binding induces allosteric changes in Nipah virus G that precede its full activation. Nat. Commun 8, 781 (2017). [PubMed: 28974687]
37. Hickey AC, "Defining the Antigenic Structure of the Henipavirus Attachment (G) Glycoprotein: Implications for the Fusion Mechanism" (UNIFORMED SERVICES UNIV OF THE HEALTH SCIENCES BETHESDA MD, 2009), (available at https://apps.dtic.mil/sti/citations/ADA538495).
38. Patel A, Weiner DB, It Takes a Matured mAb to Treat Ebolavirus Infection. Cell Host Microbe 25 (2019), pp. 10–12. [PubMed: 30629912]
39. Baum A, Fulton BO, Wloga E, Copin R, Pascal KE, Russo V, Giordano S, Lanza K, Negron N, Ni M, Wei Y, Atwal GS, Murphy AJ, Stahl N, Yancopoulos GD, Kyratsous CA, Antibody cocktail to SARS-CoV-2 spike protein prevents rapid mutational escape seen with individual antibodies. Science (2020), doi:10.1126/science.abd0831.
40. Hansen J, Baum A, Pascal KE, Russo V, Giordano S, Wloga E, Fulton BO, Yan Y, Koon K, Patel K, Chung KM, Hermann A, Ullman E, Cruz J, Rafique A, Huang T, Fairhurst J, Libertiny C, Malbec M, Lee WY, Welsh R, Farr G, Pennington S, Deshpande D, Cheng J, Watty A, Bouffard P, Babb R, Levenkova N, Chen C, Zhang B, Romero Hernandez A, Saotome K, Zhou Y, Franklin M, Sivapalasingam S, Lye DC, Weston S, Logue J, Haupt R, Frieman M, Chen G, Olson W, Murphy AJ, Stahl N, Yancopoulos GD, Kyratsous CA, Studies in humanized mice and convalescent humans yield a SARS-CoV-2 antibody cocktail. Science (2020), doi:10.1126/science.abd0827.
41. Ianevski A, Giri AK, Aittokallio T, SynergyFinder 2.0: visual analytics of multi-drug combination synergies. Nucleic Acids Res 48, W488–W493 (2020). [PubMed: 32246720]
42. Zhu Z, Dimitrov AS, Bossart KN, Crameri G, Bishop KA, Choudhry V, Mungall BA, Feng YR, Choudhary A, Zhang MY, Feng Y, Wang LF, Xiao X, Eaton BT, Broder CC, Dimitrov DS, Potent neutralization of Hendra and Nipah viruses by human monoclonal antibodies. J. Virol 80, 891–899 (2006). [PubMed: 16378991]
43. Dong J, Cross RW, Doyle MP, Kose N, Mousa JJ, Annand EJ, Borisevich V, Agans KN, Sutton R, Nargi R, Majedi M, Fenton KA, Reichard W, Bombardi RG, Geisbert TW, Crowe JE Jr, Potent Henipavirus Neutralization by Antibodies Recognizing Diverse Sites on Hendra and Nipah Virus Receptor Binding Protein. Cell. 183, 1536–1550.e17 (2020). [PubMed: 33306954]
44. Bianchi M, Turner HL, Nogal B, Cottrell CA, Oyen D, Pauthner M, Bastidas R, Nedellec R, McCoy LE, Wilson IA, Burton DR, Ward AB, Hangartner L, Electron-microscopy-based Epitope mapping defines specificities of polyclonal antibodies elicited during HIV-1 BG505 envelope trimer immunization. Immunity. 49, 288–300.e8 (2018). [PubMed: 30097292]
45. Boyoglu-Barnum S, Ellis D, Gillespie RA, Hutchinson GB, Park Y-J, Moin SM, Acton OJ, Ravichandran R, Murphy M, Pettie D, Matheson N, Carter L, Creanga A, Watson MJ, Kephart S, Ataca S, Vaile JR, Ueda G, Crank MC, Stewart L, Lee KK, Guttman M, Baker D, Mascola JR, Veesler D, Graham BS, King NP, Kanekiyo M, Quadrivalent influenza nanoparticle vaccines induce broad protection. Nature (2021), doi:10.1038/s41586-021-03365-x.

46. Barnes CO, West AP Jr, Huey-Tubman KE, Hoffmann MAG, Sharaf NG, Hoffman PR, Koranda N, Gristick HB, Gaebler C, Muecksch F, Lorenzi JCC, Finkin S, Hägglöf T, Hurley A, Millard KG, Weisblum Y, Schmidt F, Hatziioannou T, Bieniasz PD, Caskey M, Robbiani DF, Nussenzweig MC, Bjorkman PJ, Structures of Human Antibodies Bound to SARS-CoV-2 Spike Reveal Common Epitopes and Recurrent Features of Antibodies. Cell. 182, 828–842.e16 (2020). [PubMed: 32645326]
47. McLellan JS, Chen M, Joyce MG, Sastry M, Stewart-Jones GB, Yang Y, Zhang B, Chen L, Srivatsan S, Zheng A, Zhou T, Graepel KW, Kumar A, Moin S, Boyington JC, Chuang GY, Soto C, Baxa U, Bakker AQ, Spits H, Beaumont T, Zheng Z, Xia N, Ko SY, Todd JP, Rao S, Graham BS, Kwong PD, Structure-based design of a fusion glycoprotein vaccine for respiratory syncytial virus. Science. 342, 592–598 (2013). [PubMed: 24179220]
48. Marcandalli J, Fiala B, Ols S, Perotti M, de van der Schueren W, Snijder J, Hodge E, Benhaim M, Ravichandran R, Carter L, Sheffler W, Brunner L, Lawrenz M, Dubois P, Lanzavecchia A, Sallusto F, Lee KK, Veesler D, Correnti CE, Stewart LJ, Baker D, Lore K, Perez L, King NP, Induction of Potent Neutralizing Antibody Responses by a Designed Protein Nanoparticle Vaccine for Respiratory Syncytial Virus. Cell. 176, 1420–1431 e17 (2019). [PubMed: 30849373]
49. Pallesen J, Wang N, Corbett KS, Wrapp D, Kirchdoerfer RN, Turner HL, Cottrell CA, Becker MM, Wang L, Shi W, Kong WP, Andres EL, Kettenbach AN, Denison MR, Chappell JD, Graham BS, Ward AB, McLellan JS, Immunogenicity and structures of a rationally designed prefusion MERS-CoV spike antigen. Proc. Natl. Acad. Sci. U. S. A 114, E7348–E7357 (2017). [PubMed: 28807998]
50. Hsieh CL, Goldsmith JA, Schaub JM, DiVenere AM, Kuo HC, Javanmardi K, Le KC, Wrapp D, Lee AG, Liu Y, Chou CW, Byrne PO, Hjorth CK, Johnson NV, Ludes-Meyers J, Nguyen AW, Park J, Wang N, Amengor D, Lavinder JJ, Ippolito GC, Maynard JA, Finkelstein IJ, McLellan JS, Structure-based design of prefusion-stabilized SARS-CoV-2 spikes. Science (2020), doi:10.1126/science.abd0826.
51. Arunachalam PS, Walls AC, Golden N, Atyeo C, Fischinger S, Li C, Aye P, Navarro MJ, Lai L, Edara VV, Röltgen K, Rogers K, Shirreff L, Ferrell DE, Wrenn S, Pettie D, Kraft JC, Miranda MC, Kepl E, Sydeman C, Brunette N, Murphy M, Fiala B, Carter L, White AG, Trisal M, Hsieh C-L, Russell-Lodrigue K, Monjure C, Dufour J, Spencer S, Doyle-Meyer L, Bohm RP, Maness NJ, Roy C, Plante JA, Plante KS, Zhu A, Gorman MJ, Shin S, Shen X, Fontenot J, Gupta S, O'Hagan DT, Van Der Most R, Rappuoli R, Coffman RL, Novack D, McLellan JS, Subramaniam S, Montefiori D, Boyd SD, Flynn JL, Alter G, Villinger F, Kleanthous H, Rappaport J, Suthar MS, King NP, Veesler D, Pulendran B, Adjuvanting a subunit COVID-19 vaccine to induce protective immunity. Nature (2021), doi:10.1038/s41586-021-03530-2.
52. Wrapp D, Wang N, Corbett KS, Goldsmith JA, Hsieh CL, Abiona O, Graham BS, McLellan JS, Cryo-EM structure of the 2019-nCoV spike in the prefusion conformation. Science. 367, 1260–1263 (2020). [PubMed: 32075877]
53. Walls AC, Park YJ, Tortorici MA, Wall A, McGuire AT, Veesler D, Structure, Function, and Antigenicity of the SARS-CoV-2 Spike Glycoprotein. Cell. 181, 281–292.e6 (2020). [PubMed: 32155444]
54. McCallum M, Walls AC, Bowen JE, Corti D, Veesler D, Structure-guided covalent stabilization of coronavirus spike glycoprotein trimers in the closed conformation. Nat. Struct. Mol. Biol (2020), doi:10.1038/s41594-020-0483-8.
55. Corbett KS, Edwards DK, Leist SR, Abiona OM, Boyoglu-Barnum S, Gillespie RA, Himansu S, Schäfer A, Ziwawo CT, DiPiazza AT, Dinnon KH, Elbashir SM, Shaw CA, Woods A, Fritch EJ, Martinez DR, Bock KW, Minai M, Nagata BM, Hutchinson GB, Wu K, Henry C, Bahl K, Garcia-Dominguez D, Ma L, Renzi I, Kong W-P, Schmidt SD, Wang L, Zhang Y, Phung E, Chang LA, Loomis RJ, Altaras NE, Narayanan E, Metkar M, Presnyak V, Liu C, Louder MK, Shi W, Leung K, Yang ES, West A, Gully KL, Stevens LJ, Wang N, Wrapp D, Doria-Rose NA, Stewart-Jones G, Bennett H, Alvarado GS, Nason MC, Ruckwardt TJ, McLellan JS, Denison MR, Chappell JD, Moore IN, Morabito KM, Mascola JR, Baric RS, Carfi A, Graham BS, SARS-CoV-2 mRNA vaccine design enabled by prototype pathogen preparedness. Nature. 586, 567–571 (2020). [PubMed: 32756549]
56. Walls AC, Fiala B, Schäfer A, Wrenn S, Pham MN, Murphy M, Tse LV, Shehata L, O'Connor MA, Chen C, Navarro MJ, Miranda MC, Pettie D, Ravichandran R, Kraft JC, Ogohara C, Palser

A, Chalk S, Lee EC, Guerriero K, Kepl E, Chow CM, Sydeman C, Hodge EA, Brown B, Fuller JT, Dinnon KH, Gralinski LE, Leist SR, Gully KL, Lewis TB, Guttman M, Chu HY, Lee KK, Fuller DH, Baric RS, Kellam P, Carter L, Pepper M, Sheahan TP, Veesler D, King NP, Elicitation of Potent Neutralizing Antibody Responses by Designed Protein Nanoparticle Vaccines for SARS-CoV-2. Cell. 183, 1367–1382.e17 (2020). [PubMed: 33160446]

57. Walls AC, Miranda MC, Schäfer A, Pham MN, Greaney A, Arunachalam PS, Navarro M-J, Tortorici MA, Rogers K, O'Connor MA, Shirreff L, Ferrell DE, Bowen J, Brunette N, Kepl E, Zepeda SK, Starr T, Hsieh C-L, Fiala B, Wrenn S, Pettie D, Sydeman C, Sprouse KR, Johnson M, Blackstone A, Ravichandran R, Ogohara C, Carter L, Tilles SW, Rappuoli R, Leist SR, Martinez DR, Clark M, Tisch R, O'Hagan DT, Van Der Most R, Van Voorhis WC, Corti D, McLellan JS, Kleanthous H, Sheahan TP, Smith KD, Fuller DH, Villinger F, Bloom J, Pulendran B, Baric R, King NP, Veesler D, Elicitation of broadly protective sarbecovirus immunity by receptor-binding domain nanoparticle vaccines. Cell (2021), doi:10.1016/j.cell.2021.09.015.
58. Cohen AA, Gnanapragasam PNP, Lee YE, Hoffman PR, Ou S, Kakutani LM, Keeffe JR, Wu H-J, Howarth M, West AP, Barnes CO, Nussenzweig MC, Bjorkman PJ, Mosaic nanoparticles elicit cross-reactive immune responses to zoonotic coronaviruses in mice. Science. 371, 735–741 (2021). [PubMed: 33436524]
59. Kanekiyo M, Joyce MG, Gillespie RA, Gallagher JR, Andrews SF, Yassine HM, Wheatley AK, Fisher BE, Ambrozak DR, Creanga A, Leung K, Yang ES, Boyoglu-Barnum S, Georgiev IS, Tsybovsky Y, Prabhakaran MS, Andersen H, Kong W-P, Baxa U, Zephir KL, Ledgerwood JE, Koup RA, Kwong PD, Harris AK, McDermott AB, Mascola JR, Graham BS, Mosaic nanoparticle display of diverse influenza virus hemagglutinins elicits broad B cell responses. Nat. Immunol 20, 362–372 (2019). [PubMed: 30742080]
60. Suloway C, Pulokas J, Fellmann D, Cheng A, Guerra F, Quispe J, Stagg S, Potter CS, Carragher B, Automated molecular microscopy: the new Leginon system. J. Struct. Biol 151, 41–60 (2005). [PubMed: 15890530]
61. Lander GC, Stagg SM, Voss NR, Cheng A, Fellmann D, Pulokas J, Yoshioka C, Irving C, Mulder A, Lau P-W, Lyumkis D, Potter CS, Carragher B, Appion: an integrated, database-driven pipeline to facilitate EM image processing. J. Struct. Biol 166, 95–102 (2009). [PubMed: 19263523]
62. Rohou A, Grigorieff N, CTFFIND4: Fast and accurate defocus estimation from electron micrographs. J. Struct. Biol 192, 216–221 (2015). [PubMed: 26278980]
63. Voss NR, Yoshioka CK, Radermacher M, Potter CS, Carragher B, DoG Picker and TiltPicker: software tools to facilitate particle selection in single particle electron microscopy. J. Struct. Biol 166, 205–213 (2009). [PubMed: 19374019]
64. Punjani A, Rubinstein JL, Fleet DJ, Brubaker MA, cryoSPARC: algorithms for rapid unsupervised cryo-EM structure determination. Nat. Methods. 14, 290–296 (2017). [PubMed: 28165473]
65. Tegunov D, Cramer P, Real-time cryo-electron microscopy data preprocessing with Warp. Nat. Methods. 16, 1146–1152 (2019). [PubMed: 31591575]
66. Zivanov J, Nakane T, Forsberg BO, Kimanius D, Hagen WJ, Lindahl E, Scheres SH, New tools for automated high-resolution cryo-EM structure determination in RELION-3. Elife. 7 (2018), doi:10.7554/eLife.42166.
67. Punjani A, Zhang H, Fleet DJ, Non-uniform refinement: adaptive regularization improves single-particle cryo-EM reconstruction. Nat. Methods. 17, 1214–1221 (2020). [PubMed: 33257830]
68. Zivanov J, Nakane T, Scheres SHW, A Bayesian approach to beam-induced motion correction in cryo-EM single-particle analysis. IUCrJ. 6, 5–17 (2019).
69. Scheres SHW, Chen S, Prevention of overfitting in cryo-EM structure determination. Nat. Methods. 9, 853–854 (2012). [PubMed: 22842542]
70. Pettersen EF, Goddard TD, Huang CC, Meng EC, Couch GS, Croll TI, Morris JH, Ferrin TE, UCSF ChimeraX: Structure visualization for researchers, educators, and developers. Protein Sci 30, 70–82 (2021). [PubMed: 32881101]
71. Emsley P, Lohkamp B, Scott WG, Cowtan K, Features and development of Coot. Acta Crystallogr. D Biol. Crystallogr. 66, 486–501 (2010). [PubMed: 20383002]

72. Frenz B, Walls AC, Egelman EH, Veesler D, DiMaio F, RosettaES: a sampling strategy enabling automated interpretation of difficult cryo-EM maps. Nat. Methods. 14, 797–800 (2017). [PubMed: 28628127]

73. Frenz B, Rämisch S, Borst AJ, Walls AC, Adolf-Bryfogle J, Schief WR, Veesler D, DiMaio F, Automatically Fixing Errors in Glycoprotein Structures with Rosetta. Structure. 27, 134–139.e3 (2019). [PubMed: 30344107]

74. Wang RY-R, Song Y, Barad BA, Cheng Y, Fraser JS, DiMaio F, Automated structure refinement of macromolecular assemblies from cryo-EM maps using Rosetta. Elife. 5 (2016), doi:10.7554/eLife.17219.

75. Lin MJ, Shean RC, Makhsous N, Greninger AL, LAVA: a streamlined visualization tool for longitudinal analysis of viral alleles. bioRxiv (2019), p. 2019.12.17.879320.

76. Bossart KN, Geisbert TW, Feldmann H, Zhu Z, Feldmann F, Geisbert JB, Yan L, Feng YR, Brining D, Scott D, Wang Y, Dimitrov AS, Callison J, Chan YP, Hickey AC, Dimitrov DS, Broder CC, Rockx B, A neutralizing human monoclonal antibody protects african green monkeys from hendra virus challenge. Sci. Transl. Med 3, 105ra103 (2011).

77. Di Rubbo A, McNabb L, Klein R, White JR, Colling A, Dimitrov DS, Broder CC, Middleton D, Lunt RA, Optimization and diagnostic evaluation of monoclonal antibody-based blocking ELISA formats for detection of neutralizing antibodies to Hendra virus in mammalian sera. J. Virol. Methods. 274, 113731 (2019). [PubMed: 31513861]

78. Playford EG, Munro T, Mahler SM, Elliott S, Safety, tolerability, pharmacokinetics, and immunogenicity of a human monoclonal antibody targeting the G glycoprotein of henipaviruses in healthy adults: a …. Lancet Infect. Dis (2020) (available at https://www.sciencedirect.com/science/article/pii/S1473309919306346?casa_token=ka5qveaT_3AAAAAA:ywo7d3wNh12BbprnZ_cvtoAfhWUtEbvspfzA5WTZZ66pA24gxkztvUJdqyVMH84YDtabl5w).

79. Zhu Z, Bossart KN, Bishop KA, Crameri G, Dimitrov AS, McEachern JA, Feng Y, Middleton D, Wang LF, Broder CC, Dimitrov DS, Exceptionally potent cross-reactive neutralization of Nipah and Hendra viruses by a human monoclonal antibody. J. Infect. Dis 197, 846–853 (2008). [PubMed: 18271743]

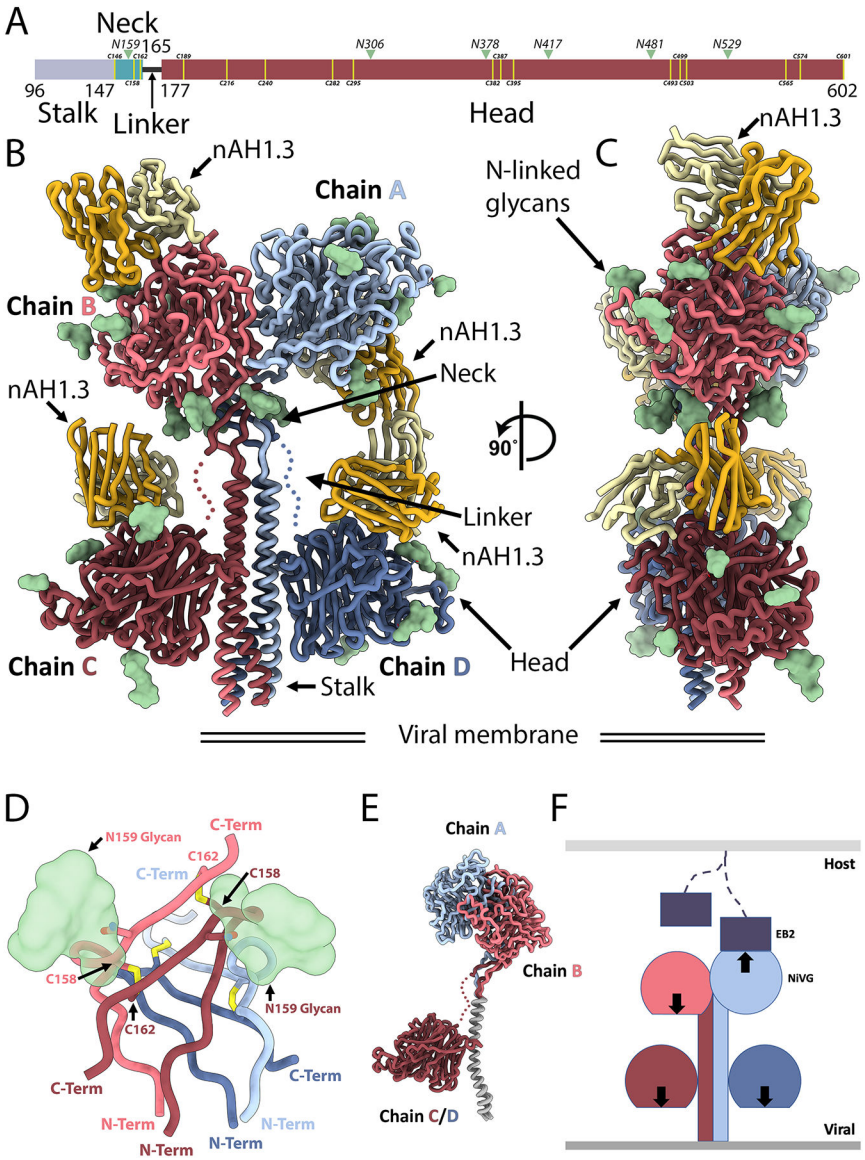

Figure 1. Architecture of the NiV G homotetramer.

(**A**) Linear representation of the NiV G ectodomain (as resolved in the cryoEM map), which contains an N-terminal stalk (residue 96 to 147), a neck domain (residue 148 to 165), a linker region (residue 166 to 177) and a C-terminal Head domain (residue 178 to 602). Green arrows indicate N-linked glycosylation sites. Yellow lines refer to cysteine residues. (**B-C**) Ribbon diagram of the NiV G ectodomain bound to the broadly neutralizing nAH1.3 Fab fragment in two orthogonal orientations. Each of the four NiV G protomers is colored distinctly and resolved N-linked glycans are rendered as green surfaces. The nAH1.3 heavy and light chains are colored gold and yellow, respectively, and only the variable domains were modeled in density. The linkers connecting the neck to the two proximal head domains are shown as dashed lines due to weaker density in the cryoEM reconstruction. (**D**) Zoomed-in view of the interlaced β-sandwich neck domain showing the four antiparallel inter-protomer disulfide bonds between residues C158 and C162 and the glycan at position

N159 protruding from the two chains shown in the foreground. (**E**) Superimposition of NiV G protomers based on the stalk highlighting that the same polypeptide chain adopts three distinct folds in the homotetrameric assembly. (**F**) Schematic representation of the NiV G homotetramer showing that only one out of four head domains orients its receptor-binding site (arrow) towards the host cell membrane (light grey) whereas the other three sites point towards the viral membrane (dark grey). EB2: ephrin-B2.

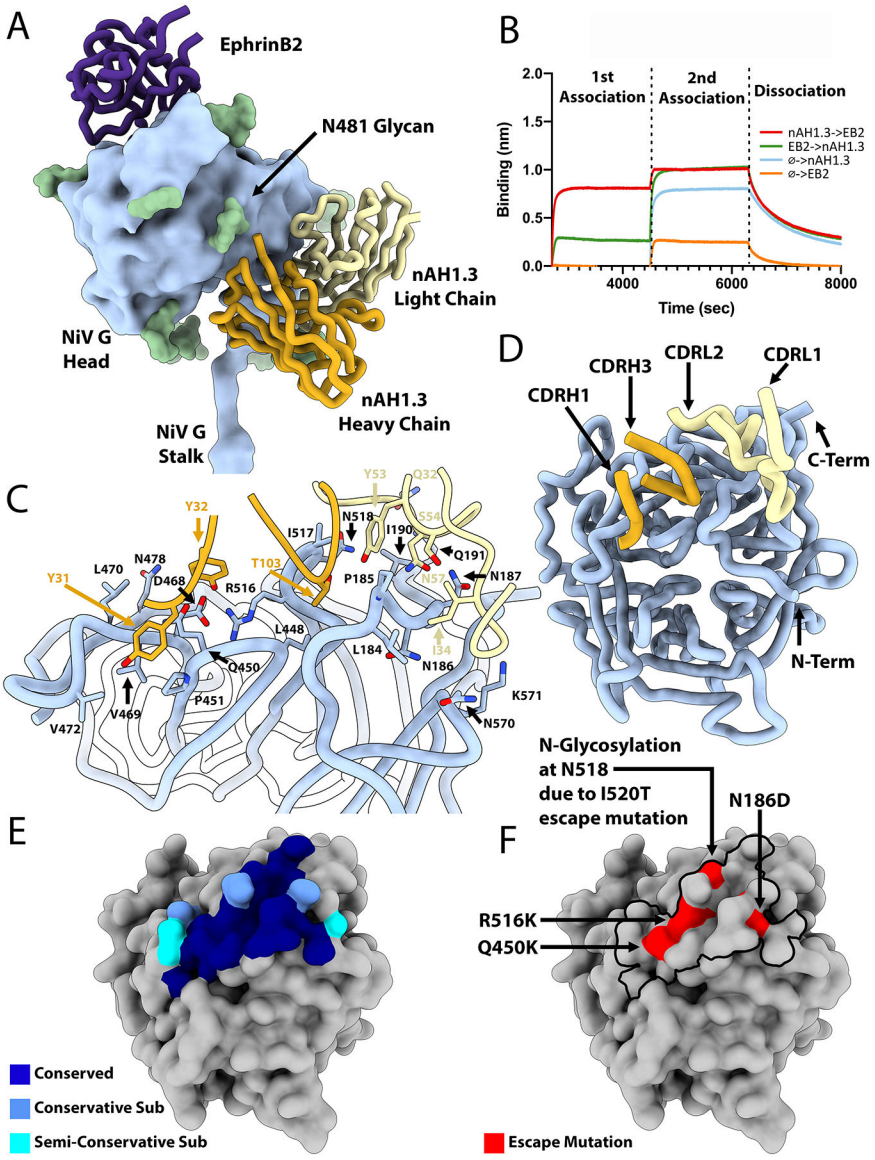

Figure 2. Structural basis for nAH1.3-mediated broad neutralization of NiV and HeV

(**A**) Superimposition of the NiV G head domain (blue surface) bound to nAH1.3 (heavy and light chains colored gold and yellow, respectively) or to ephrin-B2 (purple, PDB 2VSM) showing that they bind to opposite sides of the β-propeller (13). (**B**) Biolayer interferometry analysis of binding of the nAH1.3 Fab and ephrin-B2 (EB2) to immobilized NiV G ectodomain showing absence of competition irrespective of their order of addition. Each NiV G loaded anti-penta His biosensor probe was sequentially dipped in a solution containing 25 nM nAH1.3 Fab (red) and then 50 nM EB2 + 25 nM nAH1.3 Fab (red) or 50 nM EB2 and then 25 nM of nAH1.3 Fab + 50 nM EB2 (green). Controls with only nAH1.3 Fab (blue) or EB2 (orange) are shown for comparison. (**C**) Zoomed-in view of the interface between NiV G and nAH1.3 with selected side chains shown as sticks. (**D**) Ribbon diagram of a NiV G head domain (blue) with the interacting nAH1.3 heavy and light chains CDRs rendered in gold and yellow. (**E**) Molecular surface representation of the

NiV G head showing the nAH1.3 footprint colored by residue conservation between NiV G and HeV G. Conservative sub, conservative substitution. Semi-conservative sub, semi-conservative substitution. (**F**) Molecular surface representation of the NiV G head showing the nAH1.3 escape mutations identified here (I520T introducing an N-linked glycosylation site at position N518; N186D comes from HeV G escape mutant) and Q450K and R516K (previously described (31)).

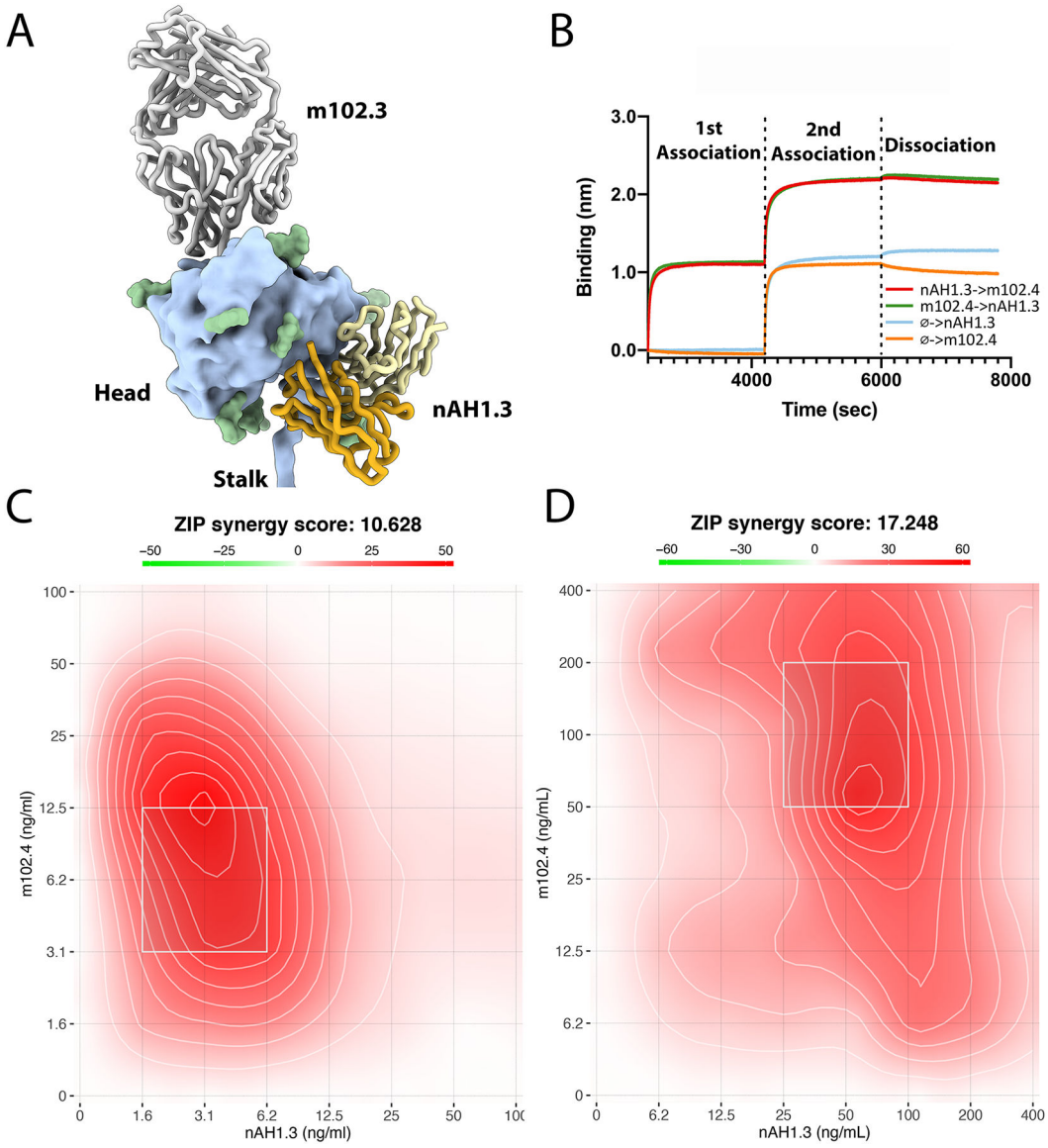

Figure 3. A HNV G head-directed mAb cocktail with synergistic neutralizing activity

(**A**) Superimposition of the NiV G head domain (blue surface) bound to nAH1.3 (heavy and light chains colored gold and yellow, respectively) or to the m102.3 Fab (heavy and light chains colored dark and light grey, respectively, PDB 6CMI) showing that they bind to opposite sides of the β-propeller. m102.3 is closely related to the m102.4 mAb. (**B**) Biolayer interferometry analysis of binding of the nAH1.3 and m102.4 IgGs to the immobilized NiV G ectodomain showing absence of competition irrespective of the order of addition. Each NiV G loaded anti-penta His biosensor probe was sequentially dipped in a solution containing 100 nM nAH1.3 IgG (red) and then 100 nM m102.4 IgG + 100 nM nAH1.3 IgG (red) or 100 nM m102.4 IgG and then 100 nM of nAH1.3 IgG + 100 nM m102.4 IgG (green). Controls with only nAH1.3 IgG (blue) or m102.4 IgG (orange) are shown for comparison. (**C-D**) Synergy maps for neutralization of replication competent rCedV-NiV-B-GFP (C) and rCedV-HeV-GFP (D) by varying concentrations of the m102.4 and nAH1.3

mAb cocktail analyzed with SynergyFinder (41). ZIP synergy score greater than 10 indicates strong synergistic relationship. The white box indicates the most synergistic region on each plot.

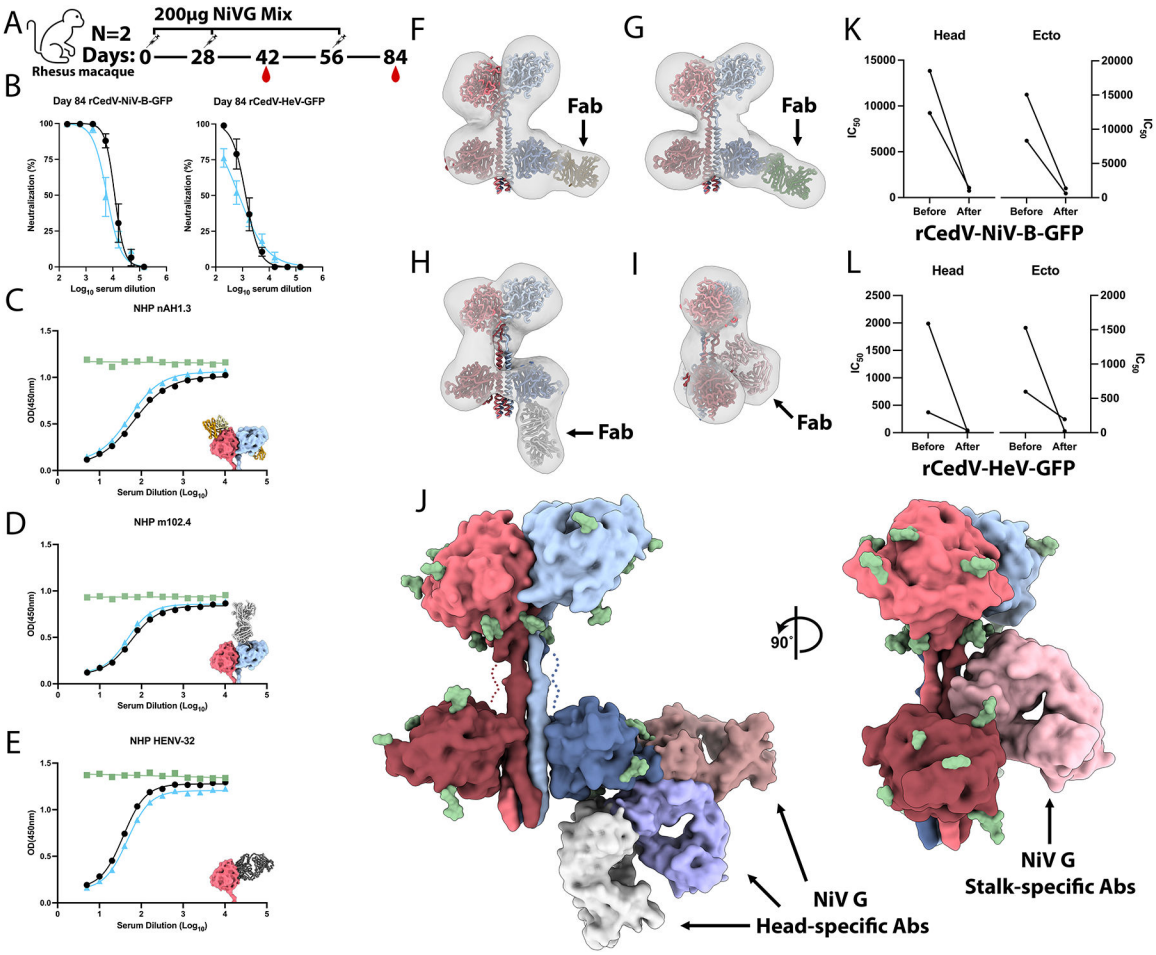

Figure 4. The NiV G receptor-binding head domain is immunodominant and accounts for most of the neutralizing activity elicited by vaccination

(**A**) Study design for vaccination of rhesus macaques, where two rhesus macaques have been immunized three times (4 weeks apart) with 200 μg of an alum-adjuvanted equimolar mixture of the purified NiV-B and NiV-M sG tetramers. Blood was collected on day 42 and day 84 post immunization. (**B**) Serum neutralizing Ab titers against rCedV-NiV-B-GFP and rCedV-HeV-GFP measured at day 84. The curves for each animal are shown in black and blue. (**C-E**) Competition ELISAs showing binding of biotinylated nAH1.3 (C), m102.4 (D) and HENV-32 (E) mAbs to the immobilized NiV G ectodomain in the presence of various dilutions of vaccine-elicited rhesus macaque sera (obtained at day 84). The curves for each animal are shown in black and blue whereas binding of the mAb in the absence of sera is shown in green (control). (**F-I**) Representative EM reconstructions (grey surfaces) of negatively stained complexes formed between purified polyclonal serum Fab fragments and NiV G fitted with atomic models for visualization of antigenic sites targeted. (**J**) Surface representation of the NiV G tetramer with three head domain-specific Fabs bound (left) and a stalk-directed Fab bound (right) highlighting antigenic sites detected in vaccine elicited polyclonal serum Abs. (**K-L**) Neutralizing Ab titers against rCedV-NiV-B-GFP (K) and

rCedV-HeV-GFP (L) before and after depletion with the NiV G head domain (Head) or the ectodomain tetramer (Ecto).